Multiscale Measurements Distinguish Cellular and Interstitial Hindrances to Diffusion In Vivo

Vikash P. Chauhan,[†‡] Ryan M. Lanning,[†§] Benjamin Diop-Frimpong,[†‡§] Wilson Mok,[†] Edward B. Brown,[¶] Timothy P. Padera,[†] Yves Boucher,[†] and Rakesh K. Jain[†*]

[†]Edwin L. Steele Laboratory, Department of Radiation Oncology, Massachusetts General Hospital and Harvard Medical School, Boston, Massachusetts 02114; [‡]Harvard School of Engineering and Applied Sciences, Harvard University, Cambridge, Massachusetts 02138; [§]Harvard-MIT Division of Health Sciences and Technology, E25-519, Cambridge, Massachusetts 02139; and [¶]Department of Biomedical Engineering, University of Rochester Medical Center, Rochester, New York 14642

ABSTRACT Molecular cancer therapy relies on interstitial diffusion for drug distribution in solid tumors. A mechanistic understanding of how tumor components affect diffusion is necessary to advance cancer drug development. Yet, because of limitations in current techniques, it is unclear how individual tissue components hinder diffusion. We developed multiscale fluorescence recovery after photobleaching (MS-FRAP) to address this deficiency. Diffusion measurements facilitated by MS-FRAP distinguish the diffusive hindrance of the interstitial versus cellular constituents in living tissue. Using multiscale diffusion measurements in vivo, we resolved the contributions of these two major tissue components toward impeding diffusive transport in solid tumors and subcutaneous tissue in mice. We further used MS-FRAP in interstitial matrix-mimetic gels and in vivo to show the influence of physical interactions between collagen and hyaluronan on diffusive hindrance through the interstitium. Through these studies, we show that interstitial hyaluronan paradoxically improves diffusion and that reducing cellularity enhances diffusive macromolecular transport in solid tumors.

INTRODUCTION

Diffusion is a significant mechanism for extravascular molecular transport in vivo, and is affected by both the viscoelasticity of the interstitial matrix and the hindrance of large bodies such as cells (1,2). These factors are important in wide-ranging normal and disease states, from extrasynaptic neuronal signaling to cancer therapy. In solid tumors, elevated interstitial pressure abrogates convective transport, limiting molecular transport to passive diffusion (3–5). However, the constituents of tumors impede the transport of nanomedicine, including antibodies, oncolytic viruses, and nanoparticles (6). A mechanistic understanding of the barriers to drug transport in a target tissue would advance the development of adjuvant therapies to potentiate cancer drugs. Yet it is currently impossible to distinguish the diffusive hindrance of interstitial matrix from that of cells to identify which components of a tissue are significant barriers to drug penetration.

No single technique currently exists for simultaneous characterization of the primary inhibitors of diffusion in living tissues: the interstitial matrix and cells. The effects of distinct interstitial matrix phases on macromolecular diffusion can be discerned with multiphoton fluorescence correlation spectroscopy (MP-FCS) (7,8), which measures on single-micron length scales, but its application in vivo is limited by sensitivity to sample movement. Multiphoton fluorescence recovery after photobleaching (MP-FRAP) (9) possesses the same resolution and is more robust to noise, giving greater potential for characterizing the nature of the interstitial phases, but its ability to measure two-phase diffusion in vivo is untested. Furthermore, these techniques cannot capture the influence of cells on bulk diffusion. Spatial Fourier analysis FRAP (SFA-FRAP) and similar methods, which quantify diffusion on length scales of tens of microns, measure diffusion properties influenced by both cells and the interstitial matrix. Yet these techniques are limited in resolution, unable to distinguish interstitial versus cellular contributions to diffusion (10). Recently developed laser-scanning FRAP techniques (11) measure diffusion in regions of scalable size; however, these measurements are dominated by diffusion along the minimum bleach dimension, generally ~5 μm. Thus, the direct effects of cell geometry on diffusion in vivo have not been quantified except in tissues with fully aligned cell anisotropies (12) or estimations based on mathematical models (13).

To address this inability to determine how each tissue component affects diffusion, we developed a multiscale approach for studying molecular diffusion in vivo that combines SFA-FRAP and MP-FRAP in an excitation-confocal manner. This method, multiscale fluorescence recovery after photobleaching (MS-FRAP), merges the advantages of both, facilitating path length-dependent diffusion measurements over multiple length scales. MS-FRAP permits diffusion measurements in vivo that simultaneously characterize the separate effects of three tissue components: two interstitial matrix phases and the cellular constituents.

Submitted January 15, 2009, and accepted for publication March 30, 2009.

Vikash P. Chauhan and Ryan M. Lanning contributed equally to this work.

*Correspondence: jain@steele.mgh.harvard.edu

Editor: Elliot L. Elson.

0006-3495/09/07/0330/7 $2.00

doi: 10.1016/j.bpj.2009.03.064

METHODS

Solution and agarose gel systems

Solutions of fluorescent probes (Sigma-Aldrich, St. Louis, MO) in deionized water are prepared from salts and filtered when necessary. Solution measurements are carried out in 50 μm path-length glass microslides (VitroCom, Mountain Lakes, NJ). Agarose gels are made by warming water or fluorophore solution to 90°C and slowly adding agarose powder (Sigma-Aldrich) to the desired concentration. To create a gel-sol interface, a mixture of 5% agarose powder in deionized water is used to partially fill a 400 μm path-length glass microslide. The microslide is then heated at 90°C until the gel becomes transparent. A solution of fluorophore is then added to the other side of the microslide to form an interface. Measurements are carried out after at least 2 h of incubation to allow partitioning of the fluorescent probe between phases. Because there is a difference in the intensity of fluorescence in the gel and sol phases caused by partitioning, the exact location of the interface is determined by measuring fluorescence photon counts on either side of the interface. The laser is gradually moved to the sample regions, where the average of these two count levels is detected at the interface. To image the bleach volumes, measurements are made in a 10% agarose gel containing 2 MDa molecular mass fluorescein isothiocyanate dextran (FITC-dextran2M) placed in a deep-well slide (VWR International, West Chester, PA). To characterize the point-spread function, a sample with fixed subresolution beads (TetraSpeck Size Kit; Molecular Probes, Eugene, OR) is used.

Animals and tumor models

Dorsal skinfold chambers (DSC) are implanted in adult male severe combined immunodeficient (SCID) mice as described previously (14). Tumor chunks are implanted in the center of the chamber 2–3 days after the initial surgery. Human soft tissue sarcoma (HSTS26T) or human colorectal adenocarcinoma (LS174T) cells are transplanted from subcutaneously grown tumors in male SCID mice. Xenotransplanted tumors are allowed to grow to at least 3.0 mm in diameter before measurements are carried out. All experiments are carried out with the approval of the Institutional Animal Care and Use Committee at the Massachusetts General Hospital.

Interstitial matrix-mimetic collagen/hyaluronan gels

Gels are formed using rat tail collagen-I (HC collagen I; BD Bioscience, San Jose, CA) and rooster comb hyaluronic acid (Sigma-Aldrich) solutions at starting concentrations of 10 mg/mL and 5.0 mg/mL, respectively. The collagen solution is first mixed with a fluorescent probe at the desired concentration. The collagen solution is then neutralized with 2.3% by volume 1 N NaOH in accordance to the manufacturer's protocol. Neutralization of the hyaluronic acid solution is attained with 10% by volume 1 N NaOH. The hyaluronic acid solution is then added to the collagen solution in the desired concentration ratio and vortexed vigorously for 7–10 s. The resulting mixture is pipetted onto glass coverslips in 30 μL drops immediately for lower-concentration gels (10 mg/mL collagen or less). For higher-concentration gels, it is centrifuged at 21,000 $\times$ g and 4°C for 15 min and then deposited. The droplets are incubated in a humidified environment at 37°C for 60 min to complete the gelation process. Gel imaging is carried out by inverting the glass coverslip onto a deep-well glass slide and sealing the contact with water. The gel droplet can then be imaged through the coverslip.

SFA-FRAP

The SFA-FRAP experiments are carried out as described previously (10), using the 488 nm-line of an Argon-ion laser (Innova 300; Coherent, Santa Clara, CA) and 40$\times$ (0.75 NA; Carl Zeiss MicroImaging, Thornwood, NY) water-immersion objective. Briefly, a mercury lamp (60010; LOT-Oriel Group, Darmstadt, Germany) is used to excite a region of the sample to be studied while images are collected with an intensified CCD camera (C-2400, Hamamatsu, Bridgewater, NJ). The sample is exposed to a brief (<200 ms), intense pulse of 488 nm laser light (800 mW) that irreversibly photobleaches fluorophores throughout the focal volume and, to an extent, the optical axis. Recovery of the fluorescence is measured by taking additional images over several minutes depending on the probe size. Diffusion coefficient values are obtained by carrying out a spatial Fourier transform of the images and fitting a model exponential recovery curve to the change in amplitude of the lowest six spatial frequencies over time with nonlinear least squares. An immobile fraction is taken into account in the model but does not affect the measured diffusion coefficient (Fig. S1 in the Supporting Material). Data acquisition and analyses are carried out using a custom code developed in LabView (National Instruments, Austin, TX). Recovery curves or spatial frequencies containing anomalies such as bleaching over time are not analyzed.

MP-FRAP

The MP-FRAP experiments are based on theory and methodology described previously (9), using a Ti:Sapphire laser (Mai-Tai Broadband; Spectra-Physics, Mountain View, CA) at 800 nm, a 40$\times$ (0.75 NA; Zeiss) water-immersion objective, and photon-counting photomultiplier tubes (H7421-40; Hamamatsu). Experiments are carried out with a custom-built multiphoton microscope containing an Axioskop upright microscope (Carl Zeiss) and Bio-Rad MRC-600 confocal laser scanner (Carl Zeiss). The laser is focused at a fixed spot (nonscanning) in the sample at low power (~5–10 mW at the sample) to monitor fluorescence without photobleaching. Photons are counted and binned using a multichannel scaler and averager (SR430, Stanford Research Systems, Sunnyvale, CA). An electro-optic modulator (KD*P Pockels' cell; ConOptics, Danbury, CT) and digital delay generator (DG535; Stanford Research Systems) rapidly modulate the laser power using custom-built hardware and a user interface developed in LabView. In a single bleaching pulse, the laser power is increased briefly (<100 μs) to a more intense pulse of light (~40–60 mW at the sample) causing irreversible photobleaching in the focal volume. The laser power is returned to the original low power and fluorescence recovery is monitored over several milliseconds, depending on the probe size. Because of the low concentration of fluorophores within the focal volume, the bleach and recovery process is repeated hundreds of times to improve signal to noise. Fractional diffusion coefficients are obtained by fitting a two-component recovery model, selected over an anomalous diffusion model based on established criteria (Fig. S2) (9), to the change in amplitude of fluorescence over time with nonlinear least-squares fitting, incorporating a trust-region algorithm using MATLAB (The MathWorks, Natick, MA). When two identical diffusion coefficients are obtained from a two-component fit, diffusion is considered to be one component with a fraction of 1.0.

MP-FCS

The MP-FCS experiments are carried out as described previously (7), using the same microscope setup as MP-FRAP. Briefly, the laser (~5–10 mW at the sample) is focused at a fixed spot in the sample. Intensity fluctuations over a period of 30–60 s measured with two photomultiplier tubes are cross-correlated via a digital correlator card (Flex02-12B; Correlator.com, Bridgewater, NJ) to determine probabilities for average residence times of probes in the focal volume. Fitting a model described previously (7) to this correlation function extracts diffusion coefficients and populations (fractions) using a nonlinear least-squares trust-region algorithm (MATLAB).

MS-FRAP measurements in gels

The gels are formulated as described with FITC-IgG at a final concentration of ~1 μM. Fifteen MS-FRAP diffusion measurements at a depth of 50 μm in random locations are made in each gel type ($n = 3$). The following procedure is used for each spot studied: 1), we image the spot using multiphoton microscopy (MPM); 2), we park the Ti:Sapphire laser along the optical axis of the microscope and carry out MP-FRAP; 3), we re-image the spot with MPM to ensure that no sample movement occurred; 4), we switch

the lasers and detectors to the SFA-FRAP light paths and perform SFA-FRAP; and 5), we again re-image the spot with MPM to ensure that no movement occurred. In extremely rare cases of sample movement, a new location is selected for measurement.

MS-FRAP measurements in vivo

Measurements are made in size-matched tumors of ~3 mm in diameter or at the center of the chamber for normal tissue. The tissues are microinjected at a depth of 500 μm with 1 μL of 1 mg/mL FITC-IgG solution at a rate of ~0.1 μL/min. Six MS-FRAP diffusion measurements at a depth of 50 μm are made at different regions in each tissue. The following procedure is used for each spot studied: 1), we image the spot using multiphoton microscopy; 2), we park the Ti:Sapphire laser along the optical axis of the microscope and collect MP-FRAP data; 3), we re-image the spot with MPM to ensure that no photodamage or sample movement occurred; 4), we switch to the light paths for SFA-FRAP and collect SFA-FRAP data; and 5), we again re-image the spot to ensure that no photodamage or sample movement occurred. In extremely rare cases of photodamage or movement, a new location is selected.

Statistical analysis

Statistical comparisons between pairs are carried out using a two-tailed Student's *t*-test. Significant differences across groups in the gel study for λ_{cell} are determined by an ANOVA (Systat; Systat Software, Chicago, IL). A probability of <0.05 was considered statistically significant for all comparisons. All data are presented as mean $\pm$ standard error (SE).

Equations

Tortuosity (λ), a measure of diffusive hindrance due to an effective increased path length (15,16), is defined as the square root of the ratio of the diffusion coefficient in free solution (D_{aq}) over that in a gel or tissue (D_{eff}):

$$\lambda = \left(D_{aq}/D_{eff}\right)^{0.5}. \quad (1)$$

(Tortuosity can alternatively be defined as a simple ratio (17,18), leading to the same end result.) Rearranging, we show that tortuosity is a proportionality factor that relates the measured effective diffusion coefficient (D_{eff}) to that in free solution (D_{aq}):

$$D_{aq} = \lambda^2 D_{eff}. \quad (2)$$

The contribution to effective diffusion at long length scales obtained using SFA-FRAP contains the effects of cell geometries, eliminating direct paths for diffusion and hindrance from interstitial matrix molecules. Thus, the tortuosity measured by SFA-FRAP (λ_{SFA}) can be considered the product of the individual tortuosities due to these factors, cellular exclusion (λ_{cell}) and interstitial matrix (λ_{int}):

$$\lambda_{SFA} = \lambda_{cell}\lambda_{int}. \quad (3)$$

The cellular hindrance (λ_{cell}) is often referred to as geometric tortuosity in the literature.

The diffusion measured by MP-FRAP at high spatial resolution within the extracellular space only probes hindrance due to the interstitial matrix. Therefore, the tortuosity quantified by MP-FRAP (λ_{MP}) is a direct measure of the interstitial tortuosity:

$$\lambda_{MP} = \lambda_{int}. \quad (4)$$

MS-FRAP directly calculates the cellular hindrance from the ratio of the SFA-FRAP and MP-FRAP tortuosities:

$$\lambda_{cell} = \lambda_{SFA}/\lambda_{MP} = \lambda_{cell}\lambda_{int}/\lambda_{int}. \quad (5)$$

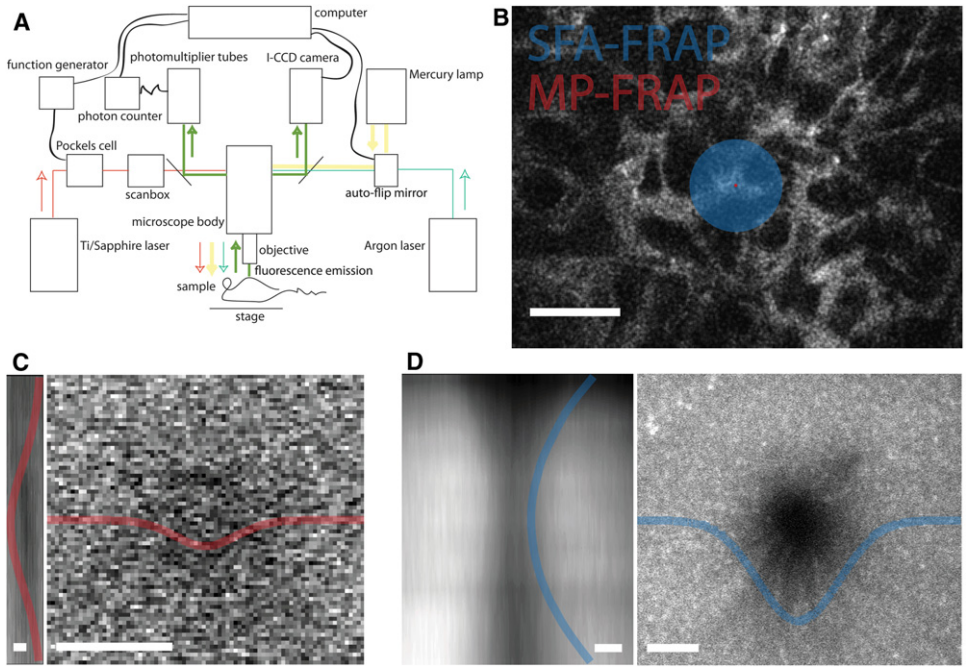

FIGURE 1 Characterization of MS-FRAP. (*A*) Experimental setup. Arrows designate directionality (*colored lines*) along optical paths. (*B*) In vivo schematic of multiscale measurement regions for each MS-FRAP component (MP-FRAP and SFA-FRAP) overlaid on an MPM image (*white*, interstitial matrix; *black*, cells). Scale bar = 30 μm. (*C* and *D*) Bleach volumes in 10% agarose containing FITC-dextran2M after a single bleach from each FRAP modality. Axial (*left*) and radial (*right*) profiles are shown with overlaid Gaussian fits. Loss of fluorescence appears where bleaching occurred. The bleach volumes at both scales are axially confocal and radially concentric. Scale bars = 1 μm in *C*, 10 μm in *D*.

RESULTS AND DISCUSSION

MS-FRAP measures multiscale diffusion in confocally concentric volumes

We developed MS-FRAP on a custom-built multiphoton microscope modified with an Argon laser for SFA-FRAP and an electro-optic modulator for MP-FRAP (Fig. 1, *A* and *B*). We determined the MP-FRAP bleach volume dimensions ($1/e^2$) as 0.540 ± 0.087 μm radially and 5.99 ± 0.34 μm axially, by multiphoton imaging after a single bleach ($n = 4$) in 10% agarose containing FITC-dextran2M (Fig. 1 *C*). By imaging subresolution fluorescent beads, the multiphoton point-spread functions ($1/e^2$) were determined to be 0.532 ± 0.146 μm radially and 3.82 ± 0.32 μm axially, slightly smaller than the bleach volume along the optical axis. The SFA-FRAP bleach volume is much larger than the multiphoton technique, with a radius of 15.9 ± 0.3 μm at the focal waist (Fig. 1 *D*). Importantly, the optical axis was identical for both techniques and Gaussian fits of the bleach volumes showed the focal planes differed by <0.5 μm (Fig. 1, *C* and *D*). We further characterized the MP-FRAP bleach volume in aqueous solution, gels, and in vivo to show that bleaching was in the nonlinear regime (two-photon) without saturation for laser powers <60 mW at the sample (Fig. S3). Additionally, photodamage was shown to occur at bleach powers >70 mW; therefore, all MP-FRAP studies in vivo used ~40 mW.

MS-FRAP measures accurate diffusion coefficients in one- or two-phase systems

We validated MS-FRAP using in vitro solution- and gel-based systems. For multiscale measurements, we defined working ranges for free FITC, FITC-IgG, and FITC-dextran (2 MDa) in solution to be concentrations above 0.1 μM (Fig. S4). Because the MP-FRAP component of MS-FRAP has a high resolution and signal/noise ratio, we investigated the ability of MP-FRAP to resolve diffusion due to two phases (Fig. 2, *A* and *B*). Using a gel (5% agarose) and solution (aqueous) interface (gel-sol) system (Fig. 2 *C*), we studied the diffusion of FITC-IgG between physical phases. For comparison, we also measured diffusion in this system with MP-FCS, whose ability to measure multicomponent diffusion is well established in vitro (19). At the gel-sol interface, both techniques were able to measure two separate

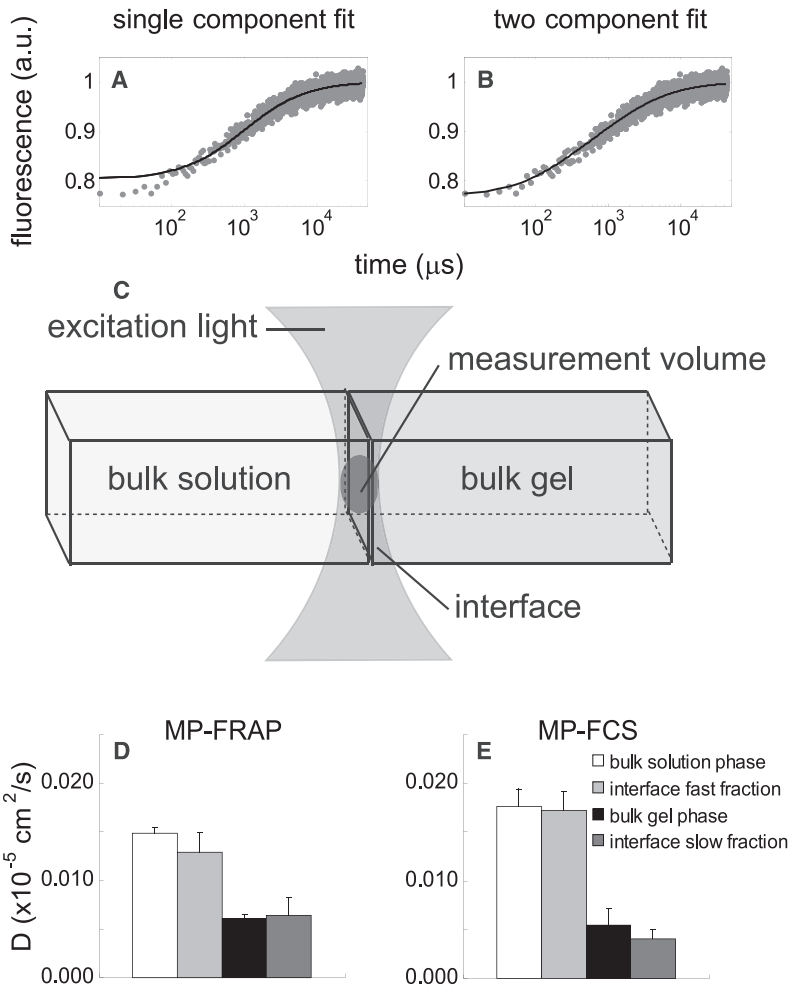

FIGURE 2 Resolving two diffusing components with MS-FRAP. (*A*) For MP-FRAP in vivo, a single-component recovery model shows poor fits at early time points. (*B*) A two-component model is able to fit recovery curves well, with lower Gaussian-distributed residuals (not shown). Accurate fitting to early time points is critical because the greatest signal/noise ratio exists during initial recovery of fluorescence. The abscissa is plotted on a logarithmic scale to highlight the temporal dynamics of the initial recovery. (*C*) Multiphoton-FRAP measured the diffusion coefficients for FITC-IgG at the interface between two physical phases (agarose gel and aqueous solution). (*D*) Diffusion coefficients at the interface determined by a two-component fluorescence recovery model were statistically indistinguishable from diffusion measured solely within either phase (gel, $p = 0.83$; solution, $p = 0.37$). (*E*) For comparison, diffusion coefficients were determined by MP-FCS, known to resolve two-component diffusion. Diffusion coefficients measured by MP-FCS at the interface are not statistically different from those shown in *D* (gel, $p = 0.28$, solution, $p = 0.15$). For each bar, $n \sim 9$.

D values statistically indistinguishable from those in pure gel and pure solution (Fig. 2, *D* and *E*). These results suggest that MP-FRAP can differentiate two diffusion coefficients separated by at least a factor of 2.

Hyaluronan enhances diffusion in collagen/hyaluronan networks

Collagen and hyaluronan are important for interstitial diffusion and may influence its two-phase properties (8), but understanding how their physical interactions determine physiological macromolecular diffusion phenomena will clarify how to overcome interstitial diffusion barriers. To explore these properties, we applied MS-FRAP in a defined in vitro system confounded by microheterogeneities (20) and in vivo. We compared diffusion of FITC-IgG in collagen/hyaluronan mixed gels with different collagen and hyaluronan content (Fig. 3, *A*, *C*, and *E*). Increasing collagen content hinders diffusion in the fast phase ($p < 0.05$, Fig. 3 *C*) and produces an increase in the slow diffusing fraction ($p < 0.01$, Fig. 3 *E*). The addition of hyaluronan to collagen gels reduced the diffusion in the fast phase as expected ($p < 0.05$, Fig. 3 *C*), but interestingly it increased the fast diffusing fraction ($p < 0.01$, Fig. 3 *E*). Thus it seems that the interactions between collagen and hyaluronan have complex effects on molecular diffusion. Increasing collagen content expands the slow phase thereby compacting and increasing viscous hindrance in the fast phase. In contrast, adding hyaluronan replaces water-filled pores, swelling the fast phase while increasing viscous hindrance. We also measured the diffusion of FITC-IgG with MS-FRAP in normal skin (subcutaneous muscle), and LS174T and HSTS26T tumors implanted in DSC in male SCID mice (Fig. 3, *B*, *D*, and *F*). SFA-FRAP measured a 3.5-fold greater diffusion coefficient in the normal versus tumor tissue ($p < 0.01$, Fig. 3 *B*), whereas MP-FRAP measured no significant difference in either phase for any tissue (Fig. 3 *D*). Measured diffusion coefficients in the two phases in gels and in vivo are similar in magnitude suggesting analogous barriers to diffusion exist at short length scales. A comparable trend of phase fractions is observed for normal tissue versus LS174T ($p < 0.05$) and for HSTS26T versus normal tissue ($p < 0.01$) and LS174T ($p < 0.05$), possibly because of differences in collagen/hyaluronan content previously reported (21–23). These comparisons indicate that the interactions of collagen and hyaluronan may play a significant role in interstitial diffusion in vivo, with the paradoxical conclusion that, unlike with collagen (24), degradation of hyaluronan may hinder diffusive transport for nanomedicine.

MS-FRAP distinguishes the interstitial and cellular contributions to diffusive hindrance

Because the influence of cells on diffusion has never been directly measured, it is unclear whether interstitial

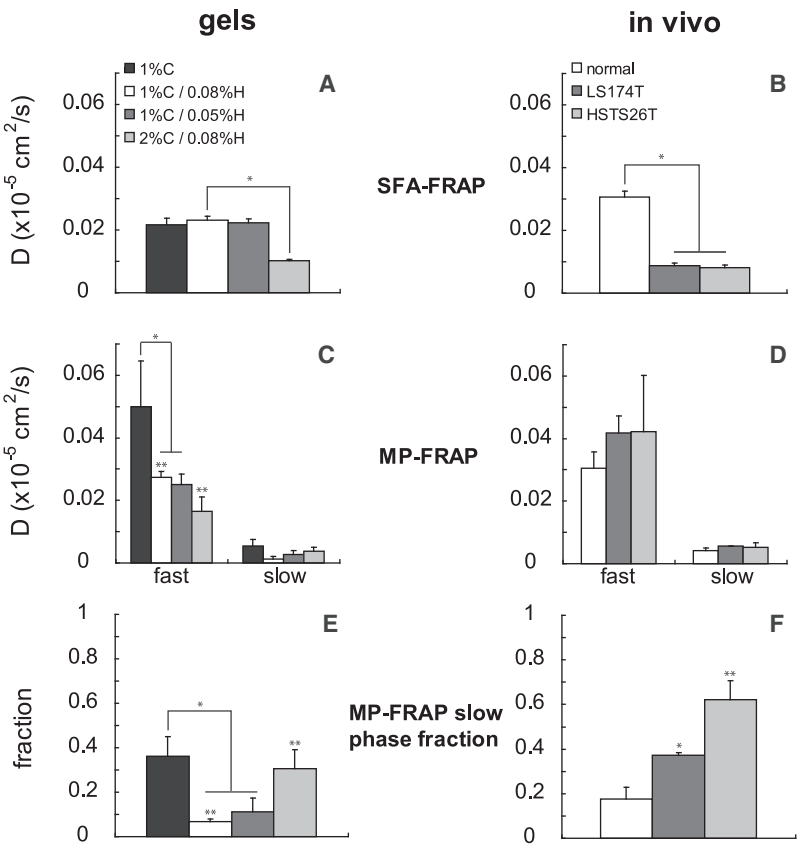

FIGURE 3 Diffusion coefficients measured by MS-FRAP in gels and in vivo. (*A*) Increasing collagen lowers the effective diffusion rate quantified by SFA-FRAP ($p < 0.01$). (*B*) SFA-FRAP shows a difference in vivo between normal and neoplastic tissue ($p < 0.01$), but not between tumor types ($p = 0.61$). (*C* and *E*) Two-component diffusion of FITC-IgG in gels at short path lengths. Generally, decreasing collagen or increasing hyaluronan content reduced the slow phase fraction, whereas the diffusion coefficients in each phase were largely unaffected. Collagen gels lacking hyaluronan demonstrated a greater diffusion coefficient in the fast phase and larger slow phase fraction. (*D* and *F*) In vivo two-component diffusion of FITC-IgG. In *D*, no significant difference is observed for either phase across tissue types. In *F*, the slow diffusing fraction shows differences between tissue types. A similar trend of phase fractions is seen as in the gels (*matched shading*), possibly due to differences in estimated collagen/hyaluronan content.

matrix or cells alone pose barriers to molecule transport in tissue. Considering the multiple length scales probed by MS-FRAP in vivo, it is apparent that the MP-FRAP component measures within the interstitial matrix (assuming no cellular uptake of fluorescent probe), whereas the SFA-FRAP component investigates regions that include several cells in addition to interstitial matrix. Recognizing this fact, we can directly measure the cellular hindrance (geometric tortuosity in the literature) of a tissue by comparing the diffusion coefficients from SFA-FRAP and MP-FRAP (weighted average of the two phases) obtained by confocal measurements (equations in Materials and Methods). The tortuosities ($\lambda = (D_{aqueous}/D_{sample})^{0.5}$) in gels on both length scales ranged from 1.5 to 1.6 for the low collagen gels to 2.5 for the high collagen gel (Fig. 4, *A* and *D*). As expected, because of their acellular nature, the cellular hindrance (ratio of the scaled tortuosities) was close to 1 ($p = 0.85$) across gels (Fig. 4 *G*).

Reducing cellularity enhances interstitial transport in vivo

To understand cellular hindrance in vivo, we determined the multiscale tortuosities for subcutaneous muscle and HSTS26T and LS174T tumors. At the tissue level, MS-FRAP measured a higher mean tortuosity in tumors and nearly equivalent tortuosity in normal tissue versus gels (Fig. 4 *B*). Within the interstitial matrix, only the soft-tissue sarcoma (HSTS26T) demonstrated a significantly higher tortuosity ($p < 0.01$) than the other tissue types possibly due to a higher collagen content (21–23) (Fig. 4 *E*). From these results, measured cellular hindrances showed diffusion in tumor tissue is further hindered by cells in contrast to gels (Fig. 4 *H*). Tumors showed greater diffusive hindrance than muscle ($p < 0.05$), where no cellular hindrance is detected given the anisotropy of muscle fibers (Fig. S5). To assess the effect of targeted cellular therapy on diffusion, we treated mice bearing LS174T tumors in the DSC with diphtheria toxin to induce apoptosis of the xenografted human tumor cells while leaving the murine tissue unaffected (25). Treatment showed a significant decrease in cellular hindrance from 1.49 to 1.15 ($p = 0.01$, Fig. 4 *I*). Therefore, decreasing tumor cellularity reduced the hindrance to macromolecular diffusion.

CONCLUSION

MS-FRAP facilitates the simultaneous measurement of the hindrance to transport from tissue components of different length scales, permitting characterization of multiple diffusion barriers in a given tissue. Our results suggest that the interstitial matrix and cells both hinder diffusion, and that reducing collagen levels and cell density—but not hyaluronan levels—in tumors should enhance drug transport. Therefore, tumor normalization through modulation of its

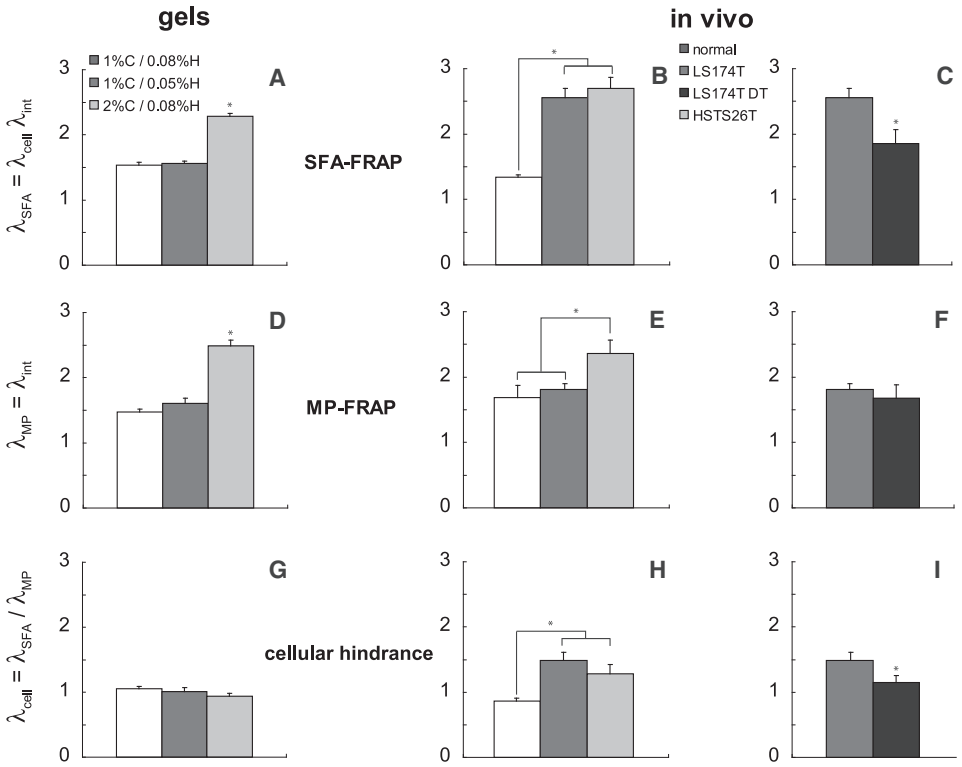

FIGURE 4 Measured tortuosity (λ) by MS-FRAP in gels and in vivo. (*A*, *B*, *D* and *E*) Path-length dependent tortuosities in interstitial matrix-mimetic gels and in vivo tissue. MP-FRAP measures diffusion in the interstitial matrix between cells while confocally concentric SFA-FRAP probes both the interstitial spaces and cellular geometries. Tortuosity >1 indicates increased hindrance to diffusion. Higher collagen content in gels increases the interstitial tortuosity (λ_{int}), or interstitial hindrance, reflected in both λ_{SFA} (*A*) and λ_{MP} (*D*) ($p < 0.01$). A similar effect is observed with λ_{MP} in *E* between tumor types previously shown to differ in collagen content ($p < 0.01$). There is a pronounced difference in λ_{SFA} between the normal tissue and the tumors shown in *B* ($p < 0.01$). (*G*) Cellular hindrance (λ_{cell}), defined as the geometric tortuosity in the literature, across gels is nonexistent ($\lambda_{cell} \sim 1$) due to acellularity ($p = 0.85$). (*H*) Diffusion in normal subcutaneous muscle demonstrates a cellular hindrance near 1 given the anisotropic arrangement of muscle fibers, whereas those in LS174T ($p < 0.01$) and HSTS26T ($p < 0.05$) are significantly greater suggesting increased cellularity. (*C*, *F* and *I*) Selective cytotoxic treatment of mice bearing LS174T tumors with diphtheria toxin showed a significant decrease in cellular hindrance ($p = 0.01$), which arises from a decrease in λ_{SFA} ($p < 0.01$) but not in λ_{MP} ($p = 0.39$) because the matrix is not affected. Tortuosity >1 indicates increased hindrance to diffusion. For each group, $n = 3$ in gels and $n = 4$ in vivo.

molecular and cellular constituents would represent a powerful strategy for improving the distribution and, in turn, effectiveness of molecular anti-cancer therapies.

Considering the advantages of the multiscale approach to studying diffusion in vivo, the MS-FRAP technique represents what we believe is a significant advance. We expect that MS-FRAP will be applicable in numerous fields from neuroscience to cancer biology to facilitate highly mechanistic studies of diffusive hindrance in tissues.

SUPPORTING MATERIAL

Five figures are available at http://www.biophysj.org/biophysj/supplemental/S0006-3495(09)00890-X.

We thank Julia Kahn and Sylvie Roberge for animal model preparation, and Peigen Huang for animal care. We also thank Ming-Zher Poh for assistance with MP-FCS.

This work was supported by the National Institutes of Health (grants 5P01CA080124-08 and 2T32CA073479-11 to R.K.J.) and Department of Defense Breast Cancer Research Program (grant W81XWH-06-1-0436 to R.M.L.).

REFERENCES

1. Nandigam, R. K., and D. M. Kroll. 2007. Three-dimensional modeling of the brain's ECS by minimum configurational energy packing of fluid vesicles. *Biophys. J.* 92:3368–3378.
2. Piet, R., L. Vargova, E. Sykova, D. A. Poulain, and S. H. Oliet. 2004. Physiological contribution of the astrocytic environment of neurons to intersynaptic crosstalk. *Proc. Natl. Acad. Sci. USA.* 101:2151–2155.
3. Jain, R. K. 1994. Barriers to drug delivery in solid tumors. *Sci. Am.* 271:58–65.
4. Minchinton, A. I., and I. F. Tannock. 2006. Drug penetration in solid tumors. *Nat. Rev. Cancer.* 6:583–592.
5. Flessner, M. F. 2005. The transport barrier in intraperitoneal therapy. *Am. J. Physiol. Renal Physiol.* 288:F433–F442.
6. McKee, T. D., P. Grandi, W. Mok, G. Alexandrakis, N. Insin, et al. 2006. Degradation of fibrillar collagen in a human melanoma xenograft improves the efficacy of an oncolytic herpes simplex virus vector. *Cancer Res.* 66:2509–2513.
7. Alexandrakis, G., E. B. Brown, R. T. Tong, T. D. McKee, R. B. Campbell, et al. 2004. Two-photon fluorescence correlation microscopy reveals the two-phase nature of transport in tumors. *Nat. Med.* 10:203–207.
8. Berland, K. M., P. T. So, and E. Gratton. 1995. Two-photon fluorescence correlation spectroscopy: method and application to the intracellular environment. *Biophys. J.* 68:694–701.
9. Brown, E. B., E. S. Wu, W. Zipfel, and W. W. Webb. 1999. Measurement of molecular diffusion in solution by multiphoton fluorescence photobleaching recovery. *Biophys. J.* 77:2837–2849.
10. Berk, D. A., F. Yuan, M. Leunig, and R. K. Jain. 1993. Fluorescence photobleaching with spatial Fourier analysis: measurement of diffusion in light-scattering media. *Biophys. J.* 65:2428–2436.
11. Mazza, D., K. Braeckmans, F. Cella, I. Testa, D. Vercauteren, et al. 2008. A new FRAP/FRAPa method for three-dimensional diffusion measurements based on multiphoton excitation microscopy. *Biophys. J.* 95:3457–3469.
12. Papadopoulos, M. C., J. K. Kim, and A. S. Verkman. 2005. Extracellular space diffusion in central nervous system: anisotropic diffusion measured by elliptical surface photobleaching. *Biophys. J.* 89:3660–3668.
13. Rusakov, D. A., and D. M. Kullmann. 1998. Geometric and viscous components of the tortuosity of the extracellular space in the brain. *Proc. Natl. Acad. Sci. USA.* 95:8975–8980.
14. Leunig, M., F. Yuan, M. D. Menger, Y. Boucher, A. E. Goetz, et al. 1992. Angiogenesis, microvascular architecture, microhemodynamics, and interstitial fluid pressure during early growth of human adenocarcinoma LS174T in SCID mice. *Cancer Res.* 52:6553–6560.
15. Patlak, C. S., and J. D. Fenstermacher. 1975. Measurements of dog blood-brain transfer constants by ventriculocisternal perfusion. *Am. J. Physiol.* 229:877–884.
16. Petersen, E. E. 1958. Diffusion in a pore of varying cross section. *AIChE J.* 4:343–345.
17. Beck, R. E., and J. S. Schultz. 1972. Hindrance of solute diffusion within membranes as measured with microporous membranes of known pore geometry. *Biochim. Biophys. ACTA.* 255:273–303.
18. Schultz, J. S., and W. Armstrong. 1978. Permeability of interstitial space of muscle (rat diaphragm) to solutes of different molecular weights. *J. Pharm. Sci.* 67:696–700.
19. Hess, S. T., S. Huang, A. A. Heikal, and W. W. Webb. 2002. Biological and chemical applications of fluorescence correlation spectroscopy: a review. *Biochemistry.* 41:697–705.
20. Kosto, K. B., and W. M. Deen. 2004. Diffusivities of macromolecules in composite hydrogels. *AIChE J.* 50:2648–2658.
21. Berria, R., L. Wang, D. K. Richardson, J. Finlayson, R. Belfort, et al. 2006. Increased collagen content in insulin-resistant skeletal muscle. *Am. J. Physiol. Endocrinol. Metab.* 290:E560–E565.
22. Nugent, L. J., and R. K. Jain. 1984. Extravascular diffusion in normal and neoplastic tissues. *Cancer Res.* 44:238–244.
23. Ramanujan, S., A. Pluen, T. D. McKee, E. B. Brown, Y. Boucher, et al. 2002. Diffusion and convection in collagen gels: implications for transport in the tumor interstitium. *Biophys. J.* 83:1650–1660.
24. Netti, P. A., D. A. Berk, M. A. Swartz, A. J. Grodzinsky, and R. K. Jain. 2000. Role of extracellular matrix assembly in interstitial transport in solid tumors. *Cancer Res.* 60:2497–2503.
25. Padera, T. P., B. R. Stoll, J. B. Tooredman, D. Capen, E. di Tomaso, et al. 2004. Pathology: cancer cells compress intratumor vessels. *Nature.* 427:695.